Multimed Tools Appl
DOI 10.1007/s11042-017-4555-7

Computer-aided diagnosis system for colon abnormalities detection in wireless capsule endoscopy images

Said Charfi[1] · **Mohamed El Ansari**[1]

Received: 16 July 2016 / Revised: 30 January 2017 / Accepted: 27 February 2017

Abstract Wireless capsule endoscopy (WCE) is a novel imaging technique that can travel through human body and image the small bowel entirely. Therefore, it has been gradually adopted compared with traditional endoscopies for gastrointestinal diseases. However, the big number of the produced images by a WCE test makes their review exhaustive for the physicians. It is helpful for clinicians if we can develop a computer-aided diagnosis system for the task of identifying the images with potential problems. The aim of this paper is to automatize the process of WCE images abnormalities detection by presenting a new texture extraction scheme for pathological inflammation, polyp, and bleeding regions discrimination in WCE images. A new approach based on local binary pattern variance and discrete wavelet transform is proposed. The new textural features scheme has many advantages, e.g., it detects multi-directional characteristics and overcomes the illuminations changes in WCE images. Intensive experiments are conducted on two datasets constructed from several WCE exams. The promising results make the presented method suitable for abnormalities detection in WCE images.

Keywords Wireless capsule endoscopy · Gastrointestinal tract · Discrete wavelet transform (DWT) · Local binary pattern (LBP) · LBP variance

1 Introduction

Digestive system cancers are ones of the most origins of death [17]. Because of the invasiveness of traditional endoscopy, WCE has been adopted instead of the former one as it enables

✉ Said Charfi
charfisaid@gmail.com

Mohamed El Ansari
melansari@gmail.com

[1] LabSIV, Department of Computer Science, Faculty of Science, Ibn Zohr University, BP 8106, 80000, Agadir, Morocco

non-invasive, painless, disposable and effective diagnosis of the entire gastrointestinal (GI) tract. WCE is well tolerated by the patients, which makes it preferable by patients with suspected diseases related to small bowel when compared with other imaging modalities [36]. The WCE system consists of an ingestible pill camera (26×11mm), data recorder and computer software for interpretation. As shown in Fig. 1, WCE is a pill-shaped device which consists of a short focal-length CMOS camera, four light sources, a battery, radio transmitter and some other miniature components. After the capsule is swallowed by patient, it takes images at a speed of two frames per second (fps) [7]. The innovative endoscopic capsule travels through the GI tract capturing and wirelessly transmitting more than 55 000 frames to a recorder tied to the patient's abdomen. The whole process takes approximately 8 h until the battery of the capsule ends. Finally, the images saved in the recorder are downloaded to a computer and the physicians will be able to review the images as a video sequence and probable sources of several GI diseases can be detected.

The diagnosis process lasts a long time and often tedious for clinicians due to the huge number of images produced in one examination. The average time to review and analyze the video frames is between 45 min and 1 h 15 min. On the other hand, the GI tract abnormalities are often present in only few frames of video. Due to oversight, physicians may miss these frames. Moreover, size and distribution of the abnormalities make them difficult to be recognized by naked eyes. Therefore, computer-aided diagnosis and offline post processing are required to diminish the great burden to physicians [21, 37, 46]. As reported, WCE technology has shown great advance in dealing with GI bleeding, Crohns disease, ulcer and other diseases [9]. However, this is a challenging topic because significant features describing GI diseases are not easily identified. Furthermore, every disease in digestive tract show its own symptoms. We note that usually the same disease varies in appearance, shape and size from patient to patient and frame to frame. Finally, resolution of WCE images is only 256×256, which makes it more difficult to manage.

Many approaches based on statistical properties of the texture were investigated. An automatic tumors detection method based on color curvelet covariance statistical texture descriptors was introduced in [5]. Kodo-giannis et al. proposed a method inspired by statistical texture descriptors extracted from different color channels histograms [19]. In [3, 18, 22], methods based on gray level co-occurrence matrices and texture spectra in the achromatic and chromatic domains for each color component histogram in a selected region of interest were stated. Baopu et al. [24, 26] proposed two different texture features to differenciate ulcer regions from normal ones in patches chosen from WCE images. The first one [24] is a curvelet based rotation invariant uniform LBP. The second one [26] is a descriptor

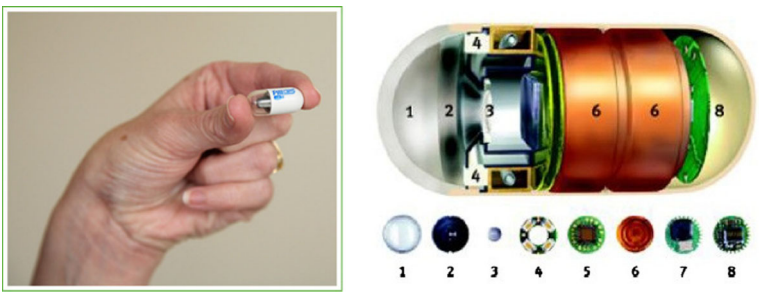

Fig. 1 (*top*) The capsule endoscopy and (*bottom*) its components (**1**) Optical dome, (**2**) lens holder (**3**), lens (**4**) illuminating LEDs, (**5**) CMOS imager, (**6**) battery, (**7**) ASIC RF transmitter, (**8**) antenna

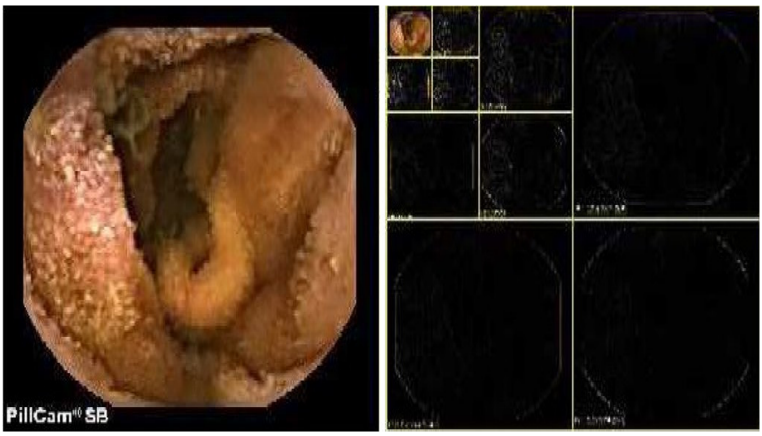

Fig. 2 (left) WCE image and (right) its corresponding three level DWT decomposition

that is built upon wavelet and LBP. The same authors [25] designed a computerized scheme aiming at polyp recognition in WCE images. This scheme utilizes a new texture feature to characterize WCE images. It integrates advantages of wavelet transform and uniform LBP with SVM as classifier. Furthermore, a method for WCE images analysis that proposes the extraction of texture information from various color models were presented in [6]. This approach aims at investigating the distribution of the structure information of abnormal and healthy tissues on RGB, HSV and CIE lab color spaces, thus, it targets color texture features. The WCE images are pre-processed using bi-dimensional ensemble empirical mode decomposition to facilitate differential lacunarity analysis to extract the texture patterns of normal and ulcerous regions. Baopu et al. [23] have proposed a method for small bowel tumor detection in WCE images using textural-based wavelet and LBP features. Recently, a saliency method based on the representation of the superpixel for ulcer detection has been presented in [41]. A WCE video segmentation to locate the boundary between small intestine, large intestine and the stomach was stated in [27]. In [16], a method for automated detection of lesion in WCE images based on color information and supervised classification of simple color vectors extracted from the neighborhood of each detected salient point. Another work based on local fuzzy patterns was proposed in [29]. Mean shift algorithm was used in [12] to detect the Crohn's disease inflammation, which is a non parametric estimator of density gradient that is employed in the joint spatial-range domain of gray level and color images for discontinuity preserving filtering and image segmentation [10]. [28] proposes a method for detecting tumor based on multi-scale curvelet and fractal dimension. The paper [32] summarizes the role of the WCE in pursuing the inflammatory disease in the bowel.

In this work, a new texture feature extraction approach is proposed. It is founded upon the discrete wavelet transformation and the LBPV. Despite the importance of the contrast in the analysis of WCE images, it is discarded in most of the state of the art approaches. In the proposed method, we take into account the variance of the local image texture which represents its contrast [20]. In the classification phase, aiming to tackle great variations of different abnormalities in WCE images, we pass through two different classifiers such as support vector machine (SVM) and multilayer perceptron (MLP) neural network. The new approach has been tested on two datasets and the results provided are satisfactory. The first

dataset is acquired from World Endoscopy Organization web site [35] and the second one is publicly available at www.capsuleendoscopy.org.

The remainder of the paper is organized as follows. Section 2 briefly introduces the DWT and LBP. Section 3 describes the proposed feature extraction scheme. In Section 4, the experiment results are presented, evaluated and compared with existing approaches. Finally, Section 5 concludes the paper.

2 Texture analysis

Texture analysis has been widely used in medical imaging field [1, 4]. In wireless capsule endoscopy images, abnormal regions show more or less differences in texture compared to their surrounding ones. This property encourages us to investigate texture features of WCE images for their analysis. Therefore, we have opted for local binary pattern operator [33], because of its popularity for texture analysis as it characterizes the spatial structure of local image texture, and the discrete wavelet transform for multi-resolution image analysis.

2.1 Local binary patterns

In this work, we utilize the well-known LBP texture operator proposed by Ojala et al. [33]. The LBP operator labels the pixels of an image by thresholding the neighborhood of each pixel and considers the result as a binary number.

The $LBP_{P,R}$ values are computed from a circularly symmetric neighbors set of P pixels on a circle of radius R. It is defined as follows:

$$LBP_{P,R} = \sum_{p=0}^{P-1} s(g_p - g_c)2^p \tag{1}$$

where s(x) is the sign function, and g_c and g_p are the values of central and neighboring pixels.

Suppose the texture image is $N \times M$. After identifying the LBP pattern of each pixel (i, j), the whole texture image can be characterized by its LBP histogram which is defined as follows:

$$H(k) = \sum_{i=1}^{N}\sum_{j=1}^{M} f(LBP_{P,R}(i, j), k), k \in [0, K] \tag{2}$$

$$f(x, y) = \begin{cases} 1, & x = y \\ 0, & otherwise \end{cases} \tag{3}$$

where K is the maximal LBP pattern value.

The $LBP_{P,R}$ operator is invariant against any gray scale monotonic transformation. It is also rotation invariant texture descriptor. In order to achieve rotation invariance and assign a unique identifier to each pattern. A rotation invariant LBP (LBP^{ri}) is introduced as follows:

$$LBP^{ri}_{P,R} = \min\{ROR(LBP_{P,R}, i) \mid i = 0, 1, ..., P - 1\} \tag{4}$$

where $ROR(x, i)$ performs a circular bit-wise right-shift i times on a P-bit LBP number x .

This operator counts the occurrence statistics of individual rotation invariant patterns representing certain micro-features in the images. In the case of P = 8 ($LBP^{ri}_{8,R}$) there are

exactly 36 patterns, which are rotation invariant, that can occur. The definition of the so-called uniform patterns is an extension to the original operator. Some LBPs are fundamental as they constitute the dominating majority, sometimes over 90 %, of all 3×3 patterns present in the observed textures. The uniform patterns are useful when we are interested in reducing the length of the feature vector and implementing a simple rotation-invariant descriptor. The fact that some binary patterns appear more frequently in texture images than others was the basis to come up with this new extension. A LBP is called uniform if, when the bit pattern is traversed circularly, the binary pattern contains at most two bitwise transitions from 0 to 1 or vice versa. For example, the patterns 11111111, 00001110 and 11100111 having 0, 2, and 2 transitions, respectively, are uniform whereas the patterns 11011001 and 01010110 having 4 and 6 transitions, respectively, are not. In the computation of the LBP labels, there is a separate label for each uniform pattern while all the non-uniform patterns are labeled with a single one. For example, when using (8, R) neighborhood, there are 256 patterns, 58 of which are uniform, which yields in 59 different labels. Considering the above discussion, a new rotation invariant operator is proposed:

$$LBP^{riu2}_{P,R} = \begin{cases} \sum_{p=0}^{P-1} s(g_p - g_c) & if \quad U(LBP_{P,R}) \leq 2 \\ P+1 & otherwise \end{cases} \tag{5}$$

where

$$\begin{aligned} U(LBP_{P,R}) = &\left|s(g_{p-1} - g_c) - (g_0 - g_c)\right| + \\ &\sum_{n=1}^{P-1} |s(g_p - g_c) - (g_{p-1} - g_c)| \end{aligned} \tag{6}$$

U is the uniformity measure which counts the spatial transitions (bitwise 0 /1 changes) in the pattern and s(x) is the sign function. The superscript riu stands for rotation invariant uniform patterns.

2.2 Multiresolution analysis

In this study, the phase of feature extraction from WCE images is performed using the DWT. In the past decades, the wavelet has been extensively utilized for texture analysis because it provides a strong method for multi-resolution image analysis [39, 40, 44, 45]. The wavelet provides information both in frequency and time domains about the signal since the use of wavelet transform is notably adequate. As has been shown in Fig. 7, the polyp, inflammation and bleeding in WCE images show great variations in size, shape and color. The wavelet can overcome this problem, hence, motivating us to turn into it [34, 42]. For a better analaysis of the mucosa of the inner GI tract, wavelet can provide zooming ability and local characterization, resulting in strong image analysis using information at different scales. DWT decomposes an image into sub-bands with their corresponding DWT coefficients. For a 2D image, DWT is implemented with a separable filter-bank on an image [30]. The DWT is implemented using cascaded filter banks in which the low pass and high pass filters satisfy certain specific constraints. h(n) and g(n) functions are, respectively, the coefficients of the low-pass and high-pass filters. We get at each level four sub-band images (LL, LH, HH, HL). The LH, HL and HH sub-bands are seen as the details components of the image. The LL sub-band is regarded as the approximation component of the image (Fig. 2). Only details components, i.e., LH, HH and HL sub-bands, provided at each level

are used in the computation of the LBPV features. In our algorithm, Daubechies three level decomposition wavelet was applied to extract the features.

3 Proposed approach

In this section, we present the new approach to extract the features describing WCE abnormalities. The derived features are provided to the classifiers, i.e., SVM and MLP, to decide which one of them is suitable for WCE analysis. We have investigated two color models (RGB and HSV) to discover which one is more efficient for abnormalities detection. The proposed approach is achieved in four main steps as depicted in Fig. 3. A WCE image taken from video capsule endoscopy is provided to the algorithm as input. The first step performs the Discrete Wavelet Transform (DWT) on the input image using three level Daubechies decomposition to get nine details components and one approximation component of the image. The second step applies the LBPV descriptor to each detailed component to provide nine LBPV histograms. In the third step, six statistical characteristics are computed for each LBPV histogram. The computed characteristics are used by the fourth step to decide whether the input capsule endoscopy image is normal or abnormal.

The rest of this section details the four steps involved in the algorithm, shown in Fig. 3, we propose for abnormalities detection from WCE images.

3.1 Discrete wavelet transform

As already explained in Section 2.2, the multiresolution analysis ability of DWT makes it suitable for revealing the significant features from WCE images. Consequently, the first step of the proposed approach consists in applying DWT to the input WCE image. For this purpose, we use three level Daubechies decomposition [2]. Figure 2 shows the results of the DWT decomposition when performed to a WCE image. Nine details components and one approximation component are obtained from the decomposition. Texture is an important feature that can be exploited to characterize WCE images because abnormal regions show differences in texture compared to their surrounding areas. The texture information is

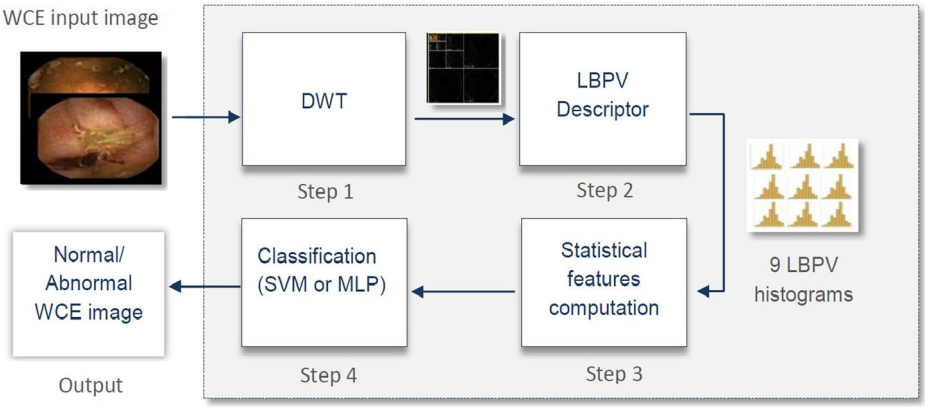

Fig. 3 Global sketch of the proposed method

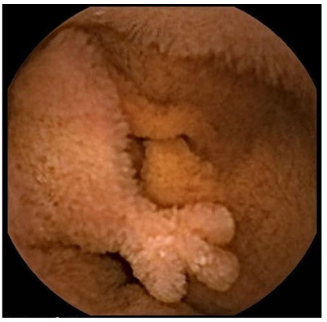

(a)

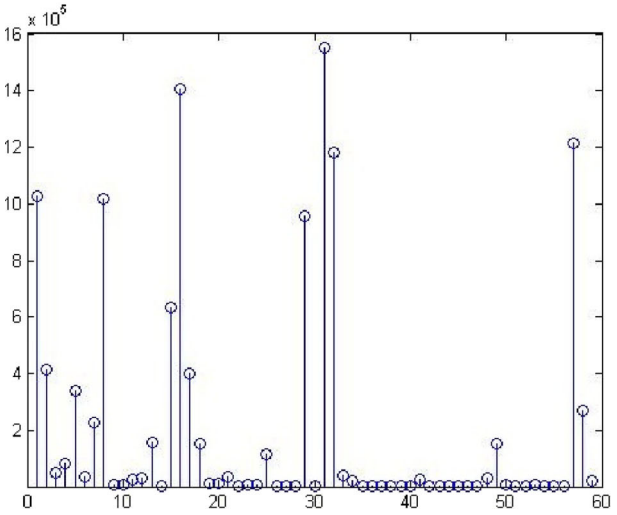

(b)

Fig. 4 WCE image with polyp and its corresponding LBPV histogram

encoded in the details components. Therefore, only the details components are used as input of the LBPV descriptor which is presented in the next subsection.

3.2 Feature extractor: LBPV

A rotation invariant measure of the local variance (VAR) can be defined as [13]

$$VAR_{P,R} = \frac{1}{P}\sum_{p=0}^{P-1}(g_p - u)^2 \tag{7}$$

where $u = 1/P\sum_{p=0}^{P-1} g_p$.

Since $LBP_{P,R}$ and $VAR_{P,R}$ are complementary, their joint distribution $LBP_{P,R}/VAR_{P,R}$ can better characterize the image local texture than using $LBP_{P,R}$ alone.

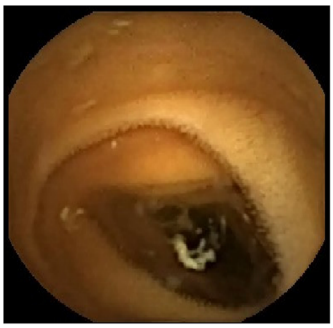

(a)

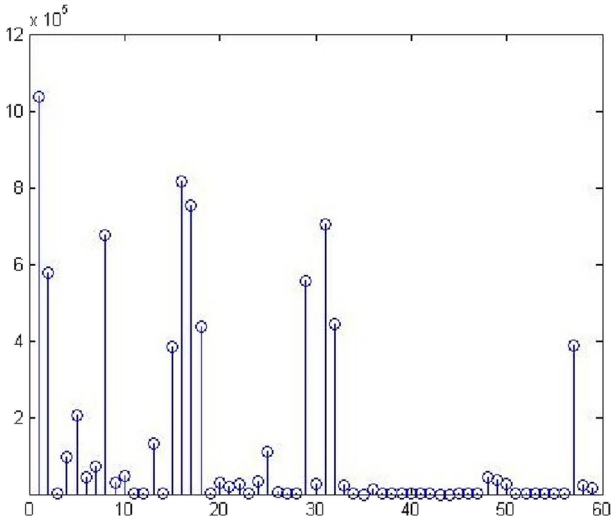

(b)

Fig. 5 Normal WCE image and its corresponding LBPV histogram

$LBP_{P,R}/VAR_{P,R}$ exploits the complementary information of local spatial pattern and local contrast [13] which makes it powerful. However, $VAR_{P,R}$ has continuous values and it has to be quantized. It is hard to obtain an optimal quantization in terms of accuracy and feature size. Consequently, the LBPV descriptor has been proposed in [13] as a solution to the above problem of $LBP_{P,R}/VAR_{P,R}$ descriptor. The LBPV is a simplified and efficient joint LBP and contrast distribution method. Therefore, enriched with contrast measures, LBPV possesses more robustness and discriminative capability than that of LBP for texture classification. It also has efficient computational complexity and possesses the same feature dimensions as those of LBP [43]. The LBP histogram is built after identifying the LBP pattern of each pixel (i, j) in an image of dimension $N \times M$ and assigning the same weight 1 to each LBP pattern no matter what the variance of the local region (Eq. 2). The variance is related to the texture feature. Usually, the high frequency texture regions will have higher variances and they contribute more to the discrimination of texture images [31]. Therefore,

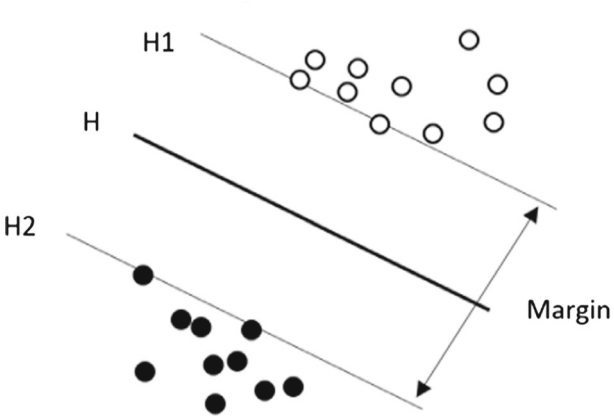

Fig. 6 The SVM binary classification

the variance $VAR_{P,R}$ can be used as an adaptive weight to adjust the contribution of the LBP code in histogram calculation. The LBPV histogram is computed as follows:

$$LBPV_{P,R}(k) = \sum_{i=1}^{N}\sum_{j=1}^{M} w(LBP_{P,R}(i,j),k), k \in [0,K] \tag{8}$$

where

$$w(LBP_{P,R}(i,j),k) = \begin{cases} VAR_{P,R}(i,j), & if\ LBP_{P,R}(i,j) = k \\ 0, & otherwise \end{cases} \tag{9}$$

Though locally operated, LBPV descriptor has an excellent ability to summarize either global or local densities in the image. As shown in Fig. 4, each density in the image is represented by a respective peak in the occurrence histogram. Therefore, LBPV can be seen as a good descriptor candidate that could eventually mirror and handle sensitively different densities in WCE images. Taking R = 1 and P = 8, the size of the vector is set to 59 ($P \times (P-1)+3$) distinct values, which is unique and independent of the image size. Here, the aforementioned values of R and P have been empirically chosen to calculate the LBPV, LBP and VAR. Figures 4 and 5 illustrate

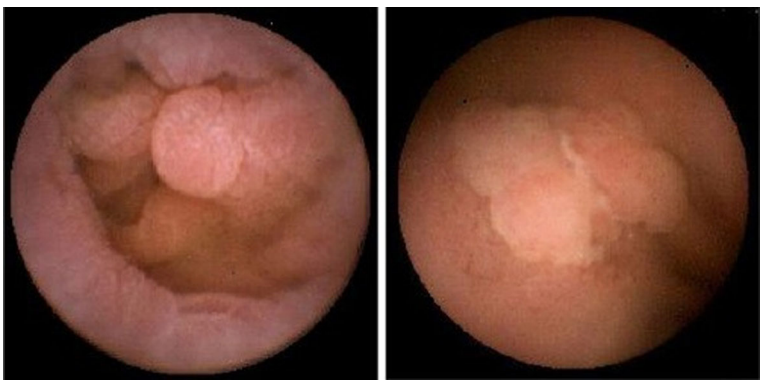

Fig. 7 Abnormal WCE images from the 1^{st} dataset

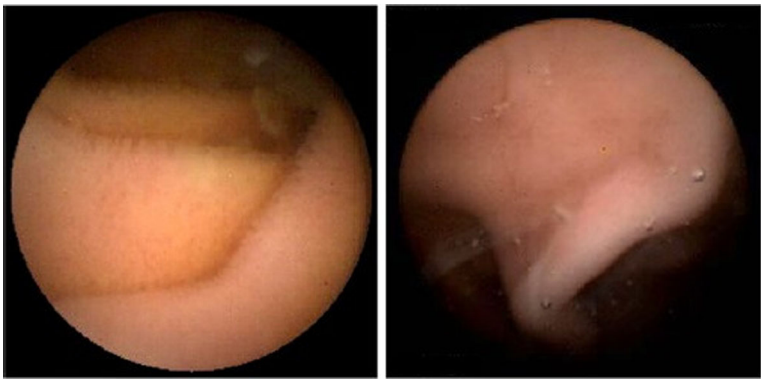

Fig. 8 Normal WCE images from the 1^{st} dataset

abnormal and normal WCE sample images together with their corresponding LBPV histograms, respectively.

We use the $LBP^{u}_{P,R}$ for the calculation of the LBPV histogram. This allows to get benefits from its advantages and reduce the computational cost by involving only the uniform patterns.

3.3 Statistical features computation

Manipulating efficiently high dimensional feature vectors is a challenging task [14]. The LBPV descriptor (Section 3.2) provides a feature vector with 59 components for each of the 9 details sub-band images. Using concatenation, the feature vector describing WCE image will have 531 (9×59) dimensions. To reduce the feature vector dimension, we propose to use 6 statistical features, mean, skew, standard deviation, entropy, kurtosis, and energy, computed from LBPV

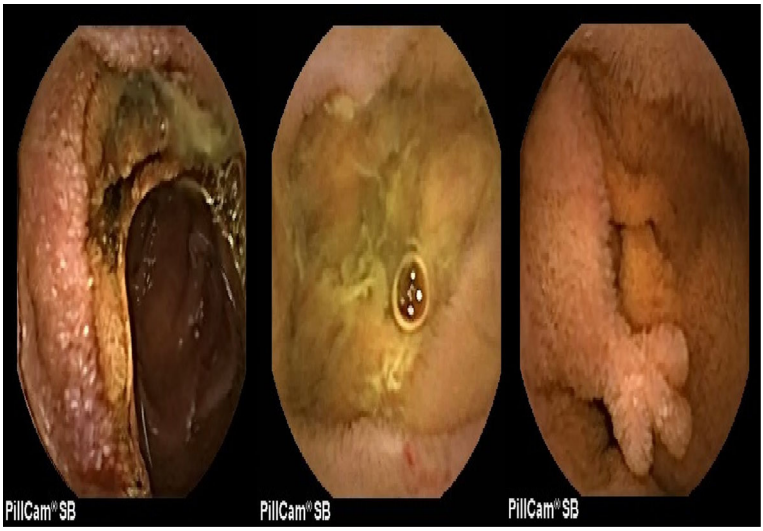

Fig. 9 Abnormal WCE images from the 2^{nd} dataset

Table 1 Classification results obtained from the 1^{st} dataset in RGB color space (%)

Classifier	Method [26]	Method [25]	LBPV
SVM Linear			
Acc	83.7	91.3	93.0
Sens	87.0	83.9	100
Spec	82.3	92.1	83.0
MLP			
Acc	82.0	92	98.6
Sens	69.0	94.7	95.8
Spec	85.0	85.7	100

histograms. Therefore, each WCE image can be characterized by a feature vector with 54 (9×6) values instead of 531.

3.4 Recognition

3.4.1 Support vector machine

SVMs were introduced first by Vapnik [38] and some extensive introductions were presented later in [8]. SVM objective is to separate the positive samples from negative ones where each sample is represented by a vector of dimension n. The basic concept of SVM is to transform the input vectors to a higher dimensional space by a nonlinear transform, and then an hyperplane which separates the data can be found. This hyperplane should be the one that has the best generalization capability. As depicted in Fig. 6, the white circles and the black circles belong to two classes and represent the training set. The hyperplane H that separates the positive samples from the negative ones is found, ensuring that the margin between the closest positives and negatives is maximal. Hyperplanes H1 and H2 are the border of each class. The data located on H1 and H2 are called support vectors. SVM is designed to solve binary classification problems. Solving multi-classes problems is accomplished through combinations of binary classification problems. There are two ways to achieve that such as one-vs.-one or one-vs.-all [11].

3.4.2 Multilayer perceptron neural network

MLP [15] is a feedforward artificial neural network model that maps sets of input data onto a set of appropriate outputs. It consists of multiple layers of nodes in a directed graph where each

Table 2 Classification results obtained from the 1^{st} dataset in HSV color space (%)

Classifier	Method [26]	Method [25]	LBPV
SVM Linear			
Acc	86.0	88.4	82.0
Sens	86.8	90.3	70.0
Spec	84.6	88.0	78.0
MLP			
Acc	91.0	88.4	97.3
Sens	85.7	90.3	95.7
Spec	92.3	88.0	95.7

Table 3 Classification results obtained from the 2^{nd} dataset in RGB color space (%)

Classifier	Method [6]	LBPV
SVM Linear		
Acc	94.3	95.29
Sens	95.5	92.20
Spec	93.1	99.5
MLP		
Acc	91.0	97.0
Sens	85.7	96.4
Spec	92.3	98.5

layer is fully connected to the next one. Except for the input nodes, each node is a neuron (or processing element) with a nonlinear activation function. MLP utilizes a well known supervised learning technique called backpropagation for training the network. It is a modification of the standard linear perceptron and can distinguish data that are not linearly separable. In this paper, traditional MLP neural network is deployed as one base classifier to analyze WCE images due to its robustness when less training data is available.

4 Experimental results

Two datasets of experimental data were built based on the image sequences acquired by WCE from different patients. The first one is composed of 100 images divided into 59 and 41 normal and abnormal WCE images, respectively. Samples of abnormal and normal WCE frames are depicted in Figs. 7 and 8, respectively. The resolution of the images is 256 × 256. The aforementioned dataset was taken from the World Endoscopy Organization web site [35]. The second one is the publicly available dataset taken from [1] and composed of 1570 WCE images extracted from 3 bleeding videos (bleeding, active bleeding and bleeding stenosis), 2 inflammatory diseases videos (enteritis infection CMV), 5 polyp videos and 3 normal videos. Examples of the frames of the second dataset are given in Fig. 9. The original images are manually labelled to provide the ground truth. The images containing any abnormal region are labelled as a positive samples; otherwise, they are labelled as a negative samples. In order to avoid over-fitting of the classification, we exploit three-fold cross-validation for all the classification experiments. The color spaces RGB and HSV have been investigated to see which one is more efficient for WCE image analysis. In order to exploit the discrimination ability of the proposed approach, we provide the features to SVM and MLP classifiers and compare their performances. The classification results are assessed in terms of the accuracy, specificity and sensitivity measures, which are defined as follows:

$$Sensitivity = \frac{Number\ of\ correct\ positive\ predictions}{Number\ of\ positives} \tag{10}$$

$$Specificity = \frac{Number\ of\ correct\ negative\ predictions}{Number\ of\ negatives} \tag{11}$$

$$Accuracy = \frac{Number\ of\ correct\ predictions}{Total\ samples} \tag{12}$$

[1] www.capsuleendoscopy.org

Table 4 Classification results obtained from the 2^{nd} dataset in HSV color space (%)

Classifier	Method [6]	LBPV
SVM Linear		
Acc	95.4	85.86
Sens	96.4	82.6
Spec	94.4	94.0
MLP		
Acc	89.0	89.43
Sens	88.7	86.6
Spec	89.7	96.5

To assess the performances of the proposed approach, it has been compared to those, dealing with the same problem, described in [6, 25, 26].

Tables 1 and 2 show the results of classification provided by the new approach and the ones presented in [25, 26] where the images of the first dataset [35] are represented in RGB and HSV color spaces. The [25, 26] were implemented and all the approaches have been tested on the same data using both SVM and MLP classifiers.

In the RGB space (Table 1), it is obvious that the proposed method outperforms the two other methods [25, 26]. Compared to the method [26], the accuracy, sensitivity and specificity have been improved by 9.3 %, 13 % and 0.7 % (resp. 16.6 %, 26.8 % and 15 %) when the SVM (resp. MLP) classifier is used. The accuracy and sensitivity have been improved by 1.7 % and 16.1 % with the SVM classifier when the new method is compared to the one in [25]. However, the last method outperforms the new one in terms of the specificity measure. Using the MLP classifier there are ameliorations of 6.6 %, 1.1 % and 14.3 % in the accuracy, sensitivity and specificity, respectively, comparing with [25].

In the HSV space (Table 2), compared to the method [26], we remark that the new method succeed in improving the accuracy, sensitivity and specificity by 6.3 %, 10 % and 3.4 % when the MLP classifier is adopted. However, it fails to do so with the SVM classifier. It needs to be improved by 4 %, 16.8 % and 6.6 %, respectively, in terms of accuracy, sensitivity and specificity to reach the performances of the former method under the SVM classifier. Similarly, the performances of the new method are 8.9 %, 5.4 % and 7.7 % better than those of the method in [25] in terms of accuracy, sensitivity and specificity using MLP. However, the new method could not reach the performances of the method [25] when the SVM classifier is adopted. We can deduce from the results detailed in Tables 1 and 2 that the features extracted by the proposed descriptor provides promising results when associated with MLP classifier and the WCE images are represented in RGB color space. Therefore, to be suited for WCE abnormalities detection, the new features should be associated with the MLP classifier and the WCE images should be represented in RGB space.

Tables 3 and 4 present the results of classification provided by the method [6] and the new one on the second dataset [1]. We note that when we adopt SVM classifier and RGB color space for the new classification method. Refereed to the method [6], the accuracy and specificity measures are improved by 0.99 % and 6.4 %, respectively, while we need an improvement of 3.3 % to reach the same sensitivity measure. Using the MLP classifier the proposed approach gives 97.0 %, 96.4 % and 98.5 % in the accuracy, sensitivity and specificity measures, respectively, with improvements of 6.0 %, 10.7 % and 6.2 % , respectively, compared to the other approach. Finally, we have compared the results of the proposed approach with the work presented in [6] in HSV color space

[1] www.capsuleendoscopy.org

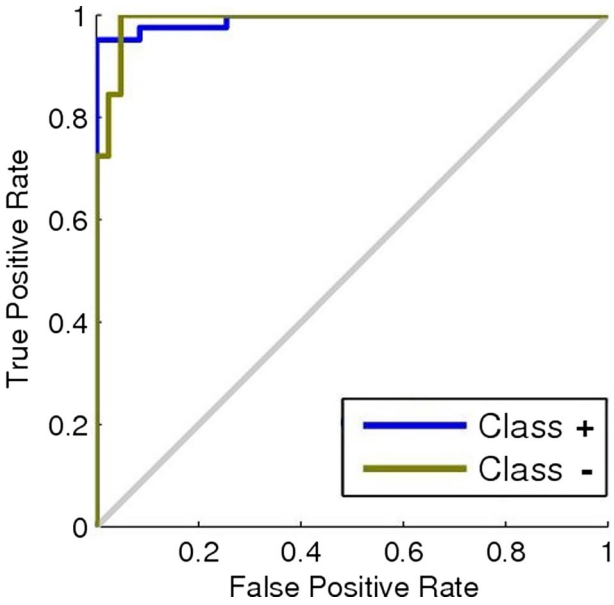

Fig. 10 ROC curve for classification applied on the 1^{st} dataset by MLP and WCE images represented in RGB

as shown in Table 4. We note that the method in [6] outperforms the new one with 9.54 %, 13.8 % and 0.4 % in all the measures using the SVM classifier. With the MLP, the performance is similar in the accuracy while the other approach delivers better in the sensitivity by 2.1 %, finally the proposed method outperforms the other approach by 6.8 % in the specificity.

Figures 10 and 11 show the Receiver Operating Characteristic (ROC) curve depicting the trade-off between the true positive rate (sensitivity) and the false positive rate (1-specificity) of

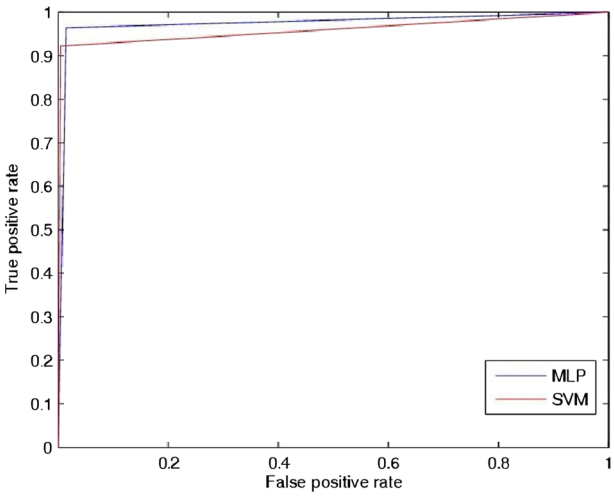

Fig. 11 ROC curve for classification applied on the 2^{nd} dataset by MLP and SVM

the recognition result given by the MLP classifier in the case of WCE images presented in RGB color space and applied to the first dataset (Fig. 10), MLP and SVM classifications results in the RGB color space using to the second dataset (Fig. 11). We have calculated the Area Under the ROC (AUC) and found it equal to 0.9714 in Fig. 10, 0.9745 for the curve in bleu color (Fig. 11) and 0.9585 for the curve in red color (Fig. 11), which can be remarked from the figures.

5 Conclusion

In this paper we have presented a novel method using wavelet based LBP for feature extraction and recognition of abnormalities in WCE images. The novel approach is constructed using DWT and LBPV descriptor leading to more description ability of the texture descriptor. The new feature descriptor is suited for WCE images analysis when it is used together with MLP classifier and the WCE images are represented in RGB color space. The experimental results prove that the proposed technique yields a good recognition rate, hence this method is effective in detecting abnormal images. However, there are still some issues and improvements that should be taken under consideration. First, the number of images should be increased in order to obtain more accurate results and conclusions. Then, more classifiers have to be used for more generalization. Some other possible work is to further study more complicated color models.

Acknowledgments We gratefully acknowledge and express our thanks to the National Center for Scientific and technical Research (CNRST) in Rabat for its research grant.

Compliance with Ethical Standards

Conflict of interests The authors declare that they have no conflict of interest.

References

1. Ahmadv A, Daliri MR (2016) A review on texture analysis methods in biomedical image processing. OMICS J Radiol
2. Akansu AN, Haddad RA (2001) Multiresolution signal decomposition: transforms, subbands, and wavelets. Academic Press
3. Ameling S, Wirth S, Paulus D, Lacey G, Vilariño F (2009) Texture-based polyp detection in colonoscopy, pp 346–350, http://dblp.uni-trier.de/db/conf/bildmed/bildmed2009.html#AmelingWPLV09
4. Barbosa DJ, Ramos J, Lima CS (2008) Detection of small bowel tumors in capsule endoscopy frames using texture analysis based on the discrete wavelet transform. In: 2008 30th annual international conference of the IEEE engineering in medicine and biology society. IEEE, pp 3012–3015
5. Barbosa DJC, Ramos J, Correia JH, Lima CS (2009) Automatic detection of small bowel tumors in capsule endoscopy based on color curvelet covariance statistical texture descriptors. In: Conference proceedings IEEE engineering in medicine and biology society, pp 6683–6686
6. Charisis VS, Hadjileontiadis LJ, Liatsos CN, Mavrogiannis CC, Sergiadis GD (2012) Capsule endoscopy image analysis using texture information from various colour models. Comput Meth Programs Biomed 107(1):61–74. http://dblp.uni-trier.de/db/journals/cmpb/cmpb107.html#CharisisHLMS12
7. Committee AT, Wang A, Banerjee S, Barth BA, Bhat YM, Chauhan S, Gottlieb KT, Konda V, Maple JT, Murad F, Pfau PR, Pleskow DK, Siddiqui UD, Tokar JL, Rodriguez SA (2013) Wireless capsule endoscopy. Gastrointest Endosc 78:805–815. doi:10.1016/j.gie.2013.06.026
8. Cristianini N, Shawe-Taylor J (2000) An introduction to support vector machines : and other kernel-based learning methods. Cambridge University Press, Cambridge, U.K., New York, Melbourne. http://opac.inria.fr/record=b1134197
9. DG A, CJ G (2003) Wireless capsule endoscopy. Hosp Physician 405(5):14–22

10. Ellahyani A, El Ansari M (2016) Mean shift and log-polar transform for road sign detection. Multimedia Tools and Applications, pp 1–19. doi:10.1007/s11042-016-4207-3

11. Ellahyani A, El Ansari M, El Jaafari I (2016) Traffic sign detection and recognition based on random forests. Appl Soft Comput 46:805–815

12. Girgis HZ, Mitchell BR, Dassopouios T, Mullin G, Haga G (2010) An intelligent system to detect crohn's disease inflammation in wireless capsule endoscopy videos. In: ISBI. IEEE, pp 1373–1376. http://dblp.uni-trier.de/db/conf/isbi/isbi2010.html#GirgisMDMH10

13. Guo Z, Zhang L, Zhang D (2010) Rotation invariant texture classification using lbp variance (lbpv) with global matching. Pattern Recogn 43(3):706–719. doi:10.1016/j.patcog.2009.08.017

14. Hafeezallah A, Abu-Bakar S (2016) Crowd counting using statistical features based on curvelet frame change detection. Multimedia Tools and Applications, pp 1–23

15. Haykin S (1998) Neural networks: a comprehensive foundation, 2nd edn. Prentice Hall PTR, Upper Saddle River, NJ, USA

16. Iakovidis DK, Koulaouzidis A (2014) Automatic lesion detection in wireless capsule endoscopy - A simple solution for a complex problem. In: 2014 IEEE international conference on image processing, ICIP 2014, Paris, France, October 27-30, 2014, pp 2236–2240. doi:10.1109/ICIP.2014.7025453

17. Iddan G, Meron G, Glukhovsky A, Swain P (2000) Wireless capsule endoscopy. Nature 405(6785):405–417

18. Kodogiannis VS, Boulougoura M, Lygouras JN, Petrounias I (2007) A neuro-fuzzy-based system for detecting abnormal patterns in wireless-capsule endoscopic images. Neurocomputing 70(4-6):704–717. doi:10.1016/j.neucom.2006.10.024

19. Kodogiannis VS, Boulougoura M, Wadge E, Lygouras JN (2007) The usage of soft-computing methodologies in interpreting capsule endoscopy. Eng Appl Artif Intell 20(4):539–553. doi:10.1016/j.engappai.2006.09.006

20. Lam V, Phan S, Le DD, Duong DA, Satoh S (2016) Evaluation of multiple features for violent scenes detection. Multimedia Tools and Applications, pp 1–25

21. Leggett CL, Wang KK (2016) Computer-aided diagnosis in gi endoscopy: looking into the future. Gastrointest Endosc 84(5):842–844

22. Li B, Meng MQH (2009) Computer-based detection of bleeding and ulcer in wireless capsule endoscopy images by chromaticity moments. Compt Biol Med 39(2):141–147

23. Li B, Meng MQH (2009) Small bowel tumor detection for wireless capsule endoscopy images using textural features and support vector machine. In: Proceedings of the 2009 IEEE/RSJ international conference on intelligent robots and systems, IROS'09. IEEE Press, Piscataway, NJ, USA, pp 498–503. http://dl.acm.org/citation.cfm?id=1733343.1733454

24. Li B, Meng MQH (2009c) Texture analysis for ulcer detection in capsule endoscopy images. Image Vis Comput 27(9):1336–1342. doi:10.1016/j.imavis.2008.12.003

25. Li B, Meng MQH (2012) Automatic polyp detection for wireless capsule endoscopy images. Expert Syst Appl 39(12):10,952–10,958. http://dblp.uni-trier.de/db/journals/eswa/eswa39.html#LiM12

26. Li B, Meng MQH, Lau JYW (2011) Computer-aided small bowel tumor detection for capsule endoscopy. Artif Intell Med 52(1):11–16. http://dblp.uni-trier.de/db/journals/artmed/artmed52.html#LiML11

27. Li B, Xu G, Zhou R, Wang T (2015) Computer aided wireless capsule endoscopy video segmentation. Med Phys 42:645–652. doi:10.1118/1.4905164

28. Liu G, Yan G, Kuang S, Wang Y (2016) Detection of small bowel tumor based on multi-scale curvelet analysis and fractal technology in capsule endoscopy. Comput Biol Med 70:131–138

29. Maghsoudi OH, Soltanian-Zadeh H (2013) Detection of abnorMalities in wireless capsule endoscopy frames using local fuzzy patterns. In: 2013 IEEE 20th Iranian Conference on Biomedical Engineering, ICBME 2013, Tehran, Iran, December 18-20, 2013, pp 286–291

30. Mallat SG (1989) A theory for multiresolution signal decomposition: the wavelet representation. IEEE Trans Pattern Anal Mach Intell 11:674–693

31. Manjunath BS, Ma WY (1996) Texture features for browsing and retrieval of image data. IEEE Trans Pattern Anal Mach Intell 18(8):837–842

32. Mitselos IV, Christodoulou DK, Katsanos KH, Tsianos EV (2015) Role of wireless capsule endoscopy in the follow-up of inflammatory bowel disease. World J Gastrointest Endosc 7:643–651. doi:10.4253/wjge.v7.i6.643
33. Ojala T, Pietikäinen M, Mäenpää T (2002) Multiresolution gray-scale and rotation invariant texture classification with local binary patterns. IEEE Trans Pattern Anal Mach Intell 24(7):971–987. doi:10.1109/TPAMI.2002.1017623
34. Omidyeganeh M, Ghaemmaghami S, Shirmohammadi S (2013) Application of 3d-wavelet statistics to video analysis. Multimedia Tools Appl 65(3):441–465
35. Organization WE (1962) Weo clinical endoscopy atlas. http://www.endoatlas.org/
36. Saurin JC, Beneche N, Chambon C, Pioche M (2016) Challenges and future of wireless capsule endoscopy. Clinical Endoscopy 42:26–29. doi:10.5946/ce.2016.49.1.26
37. Tourassi GD, Armato SG (2016) Medical imaging 2016: computer-aided diagnosis. In: Society of photo-optical instrumentation engineers (SPIE) conference series, vol 9785
38. Vapnik VN (1998) Statistical learning theory. Wiley-Interscience
39. Wang S, Yang X, Zhang Y, Phillips P, Yang J, Yuan TF (2015) Identification of green, oolong and black teas in China via wavelet packet entropy and fuzzy support vector machine. Entropy 17(10):6663–6682
40. Yang G, Zhang Y, Yang J, Ji G, Dong Z, Wang S, Feng C, Wang Q (2015) Automated classification of brain images using wavelet-energy and biogeography-based optimization. Applications, pp 1–17
41. Yuan Y, Wang J, Li B, Meng MQH (2015) Saliency based ulcer detection for wireless capsule endoscopy diagnosis. IEEE Trans Med Imaging 34(10):2046–2057. http://dblp.uni-trier.de/db/journals/tmi/tmi34.html#YuanWLM15
42. Zhang G, Wang W, Shin S, Hruska CB, Son SH (2015) Fourier irregularity index: a new approach to measure tumor mass irregularity in breast mammogram images. Multimedia Tools and Applications 74(11):3783–3798
43. Zhang L, Mistry K, Neoh SC, Lim CP (2016) Intelligent facial emotion recognition using moth-firefly optimization. Knowl-Based Syst 111:248–267
44. Zhang Y, Dong Z, Liu A, Wang S, Ji G, Zhang Z, Yang J (2015) Magnetic resonance brain image classification via stationary wavelet transform and generalized eigenvalue proximal support vector machine. J Med Imaging Health Informatics 5(7):1395–1403
45. Zhang Y, Dong Z, Phillips P, Wang S, Ji G, Yang J (2015) Exponential wavelet iterative shrinkage thresholding algorithm for compressed sensing magnetic resonance imaging. Inf Sci 322:115–132
46. Zhang YD, Wang SH, Liu G, Yang J (2016) Computer-aided diagnosis of abnormal breasts in mammogram images by weighted-type fractional fourier transform. Adv Mech Eng 8(2):1687814016634,243

Said Charfi received his Master degree in computer science from The University of Mysore, India in 2014. He is currently pursuing the Ph.D. degree in computer science at Ibn Zohr University, Faculty of Sciences, Agadir - Morocco. His research interests include medical image analysis, image processing, and computer vision.

Mohamed El Ansari received the M.S. and PhD degrees in computer science from Sidi Mohamed Ben Abdellah University, Fez - Morocco, in 1995 and 2000, respectively. From 2001 to 2003, he was a Postdoc Fellow in ENSEIRB, Bordeaux France and Norwegian University of Science and Technology, Trondheim Norway, respectively. In 2004, he was appointed as Assistant Professor at University of Ibn Zohr, Agadir Morocco, where he is currently a full professor. His research interests include image processing and computer vision. He was a visiting professor at INSA of Rouen, Ecole Centrale de Nantes, and Jean Monnet University Saint-Etienne all in France. In 2010, he was a Fulbright visiting scholar at the Computer Vision Laboratory, University of Nevada Reno, Nevada, USA.